Technical Sciences
Academy of Romania
www.jesi.astr.ro

Journal of Engineering Sciences and Innovation
Volume 6, Issue 4 / 2021, pp. 359 - 372
http://doi.org/10.56958/jesi.2022.6.4.359

C. Chemical Engineering, Materials Science and Engineering

Received ***10 September 2021*** *Accepted* ***19 November 2021***
Received in revised form ***14 October 2021***

Behavior at 1100°C of nickel–based alloys strengthened by MC carbides with M = Tantalum and Hafnium

DAME ASSANE KANE[1], LIONEL ARANDA[2], PATRICE BERTHOD[2,*]

[1]*Faculté des Sciences et Technologies, Université de Lorraine, Campus Victor Grignard, 54500 Vandoeuvre–lès–Nancy, France*
[2]*Institut Jean Lamour, Université de Lorraine, Campus Artem, 2 allée André Guinier, 54000 Nancy, France*

Abstract. The metallurgical principle constituted by a chromium–rich metallic matrix associated with eutectic script monocarbides represents a promising way in terms of high temperature performance. In this work, focus was done on polycrystalline nickel–based alloys reinforced by monocarbides involving both tantalum and hafnium, with as objectives exploring the microstructures that can be obtained and the metallurgical, chemical and mechanical behaviors of what they can be able. Two alloys were synthesized by foundry under inert atmosphere. Their as–cast microstructures were visualized by electron microscopy and their behavior at high temperature were explored, for the following temperature and time parameters: 1100°C and 50 hours for all tests. The obtained results show that the carbide population obtained after solidification is mainly composed of MC carbides in both cases but it is composed of MC carbides only for the alloy with more hafnium than tantalum. The morphological resistance of the MC carbides is good for the test conditions for both alloys. Concerning oxidation, a chromia–forming behavior was observed in the two cases, with furthermore an obvious good resistance against scale spallation at cooling. The oxidation–induced subsurface alloy degradations and the heat–induced bulk microstructure deteriorations were very limited. The bending tests under constant load allow the sample demonstrating good creep resistance. To summarize both alloys appeared as good bases for developing quite usable superalloys for this temperature where the high performance γ/γ' nickel–based single crystals start to encounter serious problems as consequences of the loss of their reinforcing particles.

Keywords: Nickel alloys, MC carbides, Tantalum, Hafnium, High temperature, Hot oxidation, Microstructure.

[*]Correspondence address: patrice.berthod@univ-lorraine.fr

Introduction

Aeroengines, energy–production turbines, glass–forming plants, waste incinerators and many transportation of industrial machines are all somewhere concerned by the existence of a high temperature zone. Chemical aggressivity of fluids and endured mechanical solicitations are also present simultaneously in these locations. The performance of the parts made of superalloys or metallic alloys is there of great importance for the good functioning and the sustainability. For not too high temperatures well-chosen classical superalloys, based on nickel, on nickel and iron, or on cobalt, may allow reaching lifetimes long enough. Beside Oxide Dispersion Strengthened alloys (the elaboration of which is always rather tricky), the best alloys in term of mechanical strength and of hot oxidation & corrosion resistance at elevated temperature are still the single crystalline alloys reinforced by high fraction of precipitated well-sized cuboidal gamma prime particles [1]. At the same time, thanks to the high amount in aluminum the resistance of such superalloys against oxidation by gases is remarkable [2]. The interest of these Ni–based single crystals is known from a long time [3] and the development of new version have never stopped until today [4–6]. However there is still a temperature limitation since their reinforcing precipitates tend to dissolve in the neighborhood of 1100°C and the main part of their high temperature strength is then lost. For an operating temperature of 1200°C other alloys – still rather easy to fabricate – can be considered. One can cite, for example, some cobalt–alloys in which the carbide population is exclusively made of tantalum carbides [7]. Unfortunately cobalt–based alloys, almost protected against hot oxidation and corrosion by chromium rather than aluminum, can be not oxidation–resistant enough because of limitations in chromium contents [2] due to the necessity to avoid metallurgical stabilities (e.g. risk of brittleness due to the precipitation sooner or later of sigma phase [1]). Thus, the better oxidation and corrosion resistant chromium–rich nickel matrix maybe preferred and considered for reinforcement by refractory carbides efficient to combat deformation thanks to adapted morphology and good thermal stability. It was observed, unfortunately, that tantalum carbides are not as easy to obtain and to stabilize as in cobalt–based alloys [8, 9]. In contrast, the much less usual hafnium carbides – very interesting in cobalt–based alloys [10] – may behave similarly in chromium–rich nickel–based alloys, in term of microstructure [11]. Even if they are not as strong as their Co – based cousins [12], their mechanical behavior at 1100°C appears to be potentially interesting [13]. So, the adaptation of these HfC carbides, also used in PM molybdenum alloys [14] or tungsten – based composites [15], may lead to interesting properties. Furthermore, thanks to a Ni–Cr matrix instead a Co–Cr one, their high temperature oxidation resistance can be very good [16]. The problem with hafnium is that this element is very expensive and not available in great quantity. A compromise can be found: considering that tantalum is cheaper than hafnium but not as efficient as this latter element for obtaining stable script MC carbides in nickel–based alloys, and that hafnium allows obtaining easily MC carbides even in Ni–based alloys, introducing both tantalum and

hafnium as MC–former elements may lead to nickel–based superalloys with good resistance against high temperature oxidation and creep. This is the way which will be explored in this work.

Methodology

Two alloys were elaborated and characterized to investigate the potentialities of this metallurgical principle. Their chemical compositions were defined in order to respect the following criteria:

- Containing more than 20wt.%Cr for promoting high hot oxidation and corrosion resistance (20 wt.% is usually considered as the threshold Cr content to allow nickel–based alloys to be chromia–forming)
- Containing 0.4wt.%C for obtaining a carbides network dense enough to efficiently reinforce the alloys but not too dense to avoid possible lack of ductility and toughness
- Containing tantalum and hafnium in quantities great enough to allow these elements monopolizing carbon to form only MC carbides

Two alloys were elaborated: one containing less hafnium than tantalum (called: "Hf<Ta alloy") and one containing more hafnium than tantalum (called: "Hf>Ta alloy"). Parts of pure metals and graphite (all of purity > 99.9%), bought from Alfa Aesar, were weighed and placed in the water–cooled copper crucible present inside a silica tube, itself surrounded by a water–cooled copper coil. The melting chamber was closed and an inert atmosphere made of 200mbars of pure argon was created inside. By injecting an alternative current in the coil, Foulcault's currents were induced in the metallic parts which were consequently heated by Joule effect. The applied operating parameters were: voltage increasing from 0 to 4,000 Volts, frequency equal to 110,000 Kz, heating time to achieved melting estimated to 2 minutes, holding time in the liquid state taken as 5 minutes, cooling done by decreasing voltage then natural cooling for a whole duration of about half an hour. The apparatus (CELES high frequency induction furnace, crucible, coil, silica tube and power box) before and during melting, as well one of the obtained ingots, are shown in the photographs present in Fig. 1.

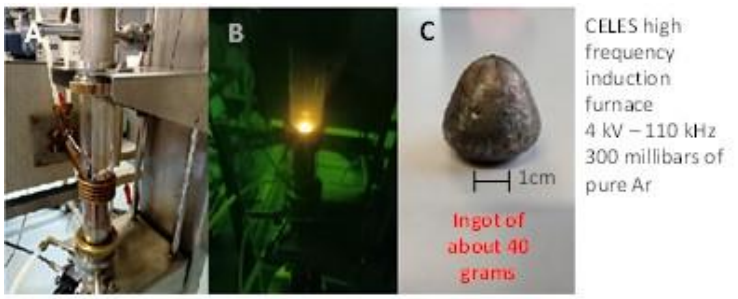

Fig. 1. The hottest part of the furnace before (A) and during melting (B); one of the obtained ingots (C).

After classical metallographic preparation (cutting of several parts, embedding, grinding, polishing until a mirror–like state), a sample per alloy was observed using a FEI Quanta 600FEG Scanning Electron Microscope (FEG–SEM) to control the obtained as–cast microstructures and the chemical compositions of both alloys (with the Energy Dispersion Spectrometry device equipping this FEG–SEM).
Per alloy again, two parallelepipeds were cut, to obtain the following approximative dimensions for the samples destined to the high temperature oxidation tests and accurate dimensions for the samples destined to the bending creep tests:

- 10 mm × 10 mm × 3 mm for the oxidation tests
- 1 mm (thickness) × 2 mm (width) × 15 mm (length) for the creep tests

The surface states of the high temperature oxidation samples as well as of the bending creep sample were initialized with #1200–grit SiC papers. The oxidation samples were additionally subjected to smoothing of their edges and corners to do not favor local overoxidation.
The oxidation samples were placed in the hot zone furnace of a SETARAM TGA92 thermobalance. Heating was carried out at 20°C per minutes until reaching 1100°C. After 50 hours spent at this temperature in a dry synthetic air (80%N_2–20%O_2) continuous flow (about 1.5 liters per hour), a cooling of -5 °C per minute was applied. The used thermobalance is illustrated by a photograph in Fig. 2.

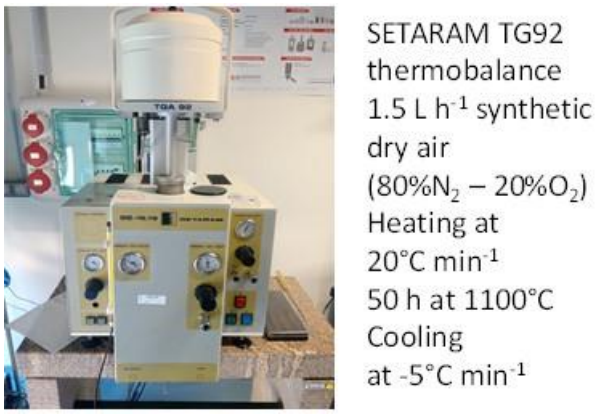

Fig. 2. The thermobalance used to carry out the oxidation tests.

The bending creep tests were performed using a TMA92-16.18 thermodilatometer especially equipped to allow performing 3–points flexural bending creep tests. The parallelepiped sample was placed on two alumina rods separated from one another by a distance of 12 mm. Another alumina piece, linked to an electronic sensor, applied a constant force on the middle of the flat top face of the creep sample. This force was rated in order to generate a maximal tensile stress equal to 20 MPa in middle of the bottom face. The test temperature continuously applied all along the

50 hours duration was 1100°C here too. The atmosphere was made of pure Ar. The location of interest in the apparatus is photographed in Fig. 3.

Fig. 3. The creep sample before introduction in the furnace and the application of the constant force.

The oxidized samples were first subjected to X-ray diffraction (Bruker D8 Advance, Fig. 4). Thereafter they were coated first with a thin gold layer, using a cathodic evaporator from JEOL. This allowed their oxides on surface being electrically conductive, allowing the observation of the surfaces of the outer scales of oxides (tungsten filament scanning electron microscope JSM 6010 LA from JEOL, WF–SEM) in the Secondary Electrons mode (SE) and in the Backscattered Electrons mode (BSE). They were thereafter coated by a thicker nickel layer by electrodeposition in a Watt's bath heated at 50°C. This outer metallic shell allowed protecting the external oxide scales during the cutting of the oxidized samples to obtain two halves in order to prepare cross–sections (embedding, grinding, polishing until a mirror–like state). These ones were characterized (imagining, concentration profiles) with the WF–SEM equipped with an EDS device for the oxidized surfaces, and oxidation–deteriorated subsurfaces and observed with the FEG–SEM for the aged bulk microstructures.

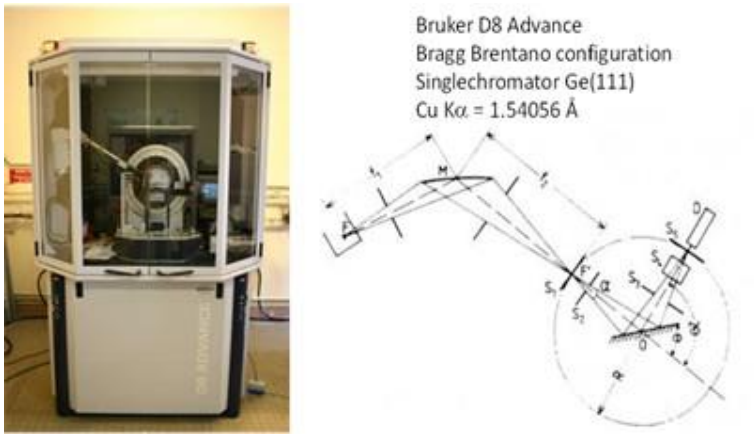

Fig. 4. The diffractometer used for the XRD characterization of the oxidized samples.

Results and discussion

As–cast microstructures and chemical compositions

Two BSE micrographs acquired using the FEG–SEM are provided in Figure 1 to illustrate the microstructures of both alloys in their as–cast states. The two alloys are composed of a dendritic matrix (grey phase) and of interdendritic carbides. The "Ta > Hf" alloy is obviously not composed of MC carbides only (the white phase) since some chromium carbides (dark) are also present. However, compared to a Hf–free Ni–30Cr–0.4C–6Ta alloy [**8**], which contains much more chromium carbides and much less MC carbides, the presence of hafnium had obviously an influence, despite its contents which is lower than the Ta one. In contrast, the carbide population in the as–cast "Hf > Ta" alloy is only made of MC carbides. No chromium carbide was evidenced.

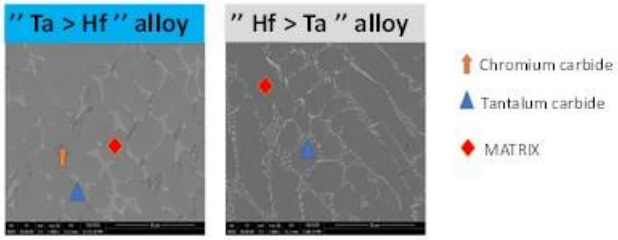

Fig. 5. The as–cast microstructures of the two alloys (FEG–SEM, BSE mode).

The chemical compositions of these two alloys were specified using by EDS with the FEG–SEM in Fig. 6 for the "Ta > Hf" alloy and in Fig. 7 for the "Hf > Ta" alloy. They are both rich enough in chromium (> 20 wt.%) to behave in oxidation at high temperature as chromia–forming alloys. Really, the "Ta > Hf" alloy is really richer in tantalum than in hafnium and the "Hf > Ta" alloy is richer in hafnium than in tantalum.

" Ta > Hf " alloy (bulk aged at 1100°C)	Ni	Cr	Hf	Ta
Average	Bal.	25.01	2.63	6.93
Std Dev	/	± 0.66	± 0.12	± 0.23

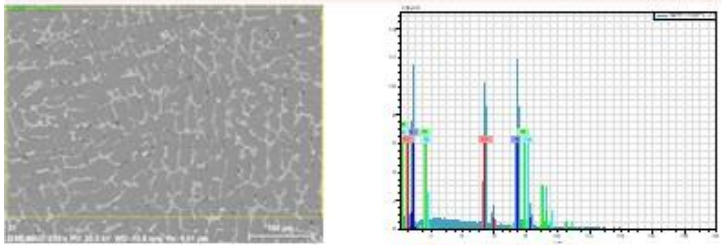

Fig. 6. Results of the full frame EDS analysis in the bulk of the "Ta > Hf" alloy; measured contents (top), analyzed area (bottom left) and corresponding EDS spectra (bottom right); FEG–SEM EDS device.

External oxide scales

Obviously the external oxide scales formed over the two oxidation samples are still present on these samples after cooling to ambient temperature. They did not suffer intense scale spallation at cooling as this was earlier observed for a Ni–30Cr–0.4C–6Ta alloy [**17**]. This latter alloy had totally lost its external oxide scale during the cooling applied at the end of the 1100°C–isothermal stage. The present alloys behave totally differently, demonstrating in contrast a much greater resistance against oxide scale spallation at cooling.

" Hf > Ta " alloy	Ni	Cr	Hf	Ta
Average	Bal.	22.70	6.07	3.71
Std Dev	/	± 0.64	± 0.22	± 0.16

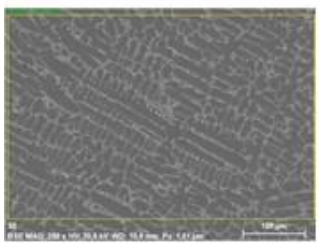

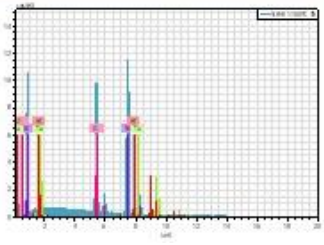

Fig. 7. Results of the full frame EDS analysis in the bulk of the "Hf > Ta" alloy; measured contents (top), analyzed area (bottom left) and corresponding EDS spectra (bottom right); FEG–SEM EDS device.

The obtained XRD spectra acquired on the oxidized surfaces prior to gold deposition (Figure 8 for the oxidized "Ta > Hf" alloy, Fig. 9 for the oxidized "Hf > Ta" alloy) clearly show that chromia is the main oxide present on both surfaces. No peak corresponding to the matrix or carbides of the substrate alloy are visible. The alloys are totally hidden by the intact continuous external chromia scale.

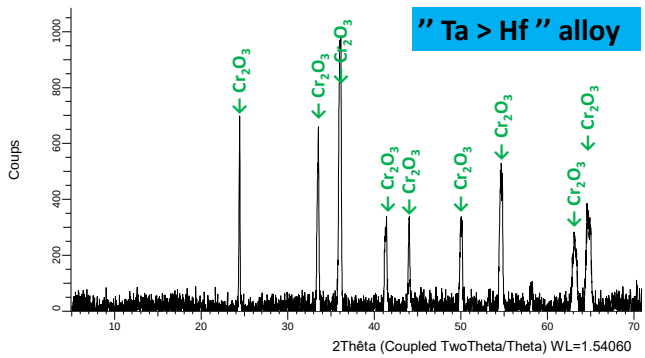

Fig. 8. Diffractogram acquired on the oxidized surface of the "Ta > Hf" alloy.

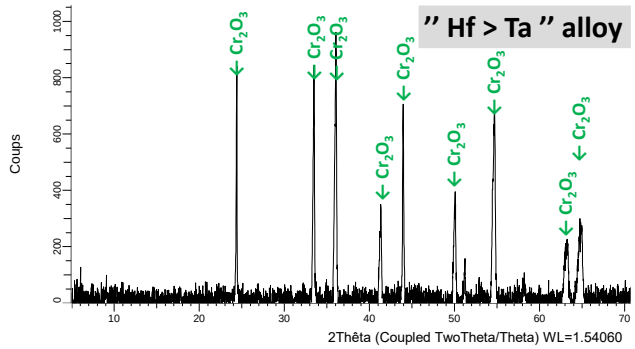

Fig. 9. Diffractogram acquired on the oxidized surface of the "Hf > Ta" alloy.

After gold–deposition the samples covered by their external oxide scales were placed in the WF–SEM to observe these scales. As observed with the nake eye and as confirmed first by the XRD diffractogram, the general and more detailed SE mode–observations of the scales clearly show that no part of scale was lost during cooling and even room temperature handling (Fig. 10). The comparison of the SE micrographs recorded on the two oxidized alloys for a same magnification suggests that the external face of the scale is a little coarser for the "Ta > Hf" alloy than for the "Hf > Ta" alloy. Looking at the BSE–micrographs (Fig. 11) leads to the same feeling. This suggests that hafnium – element more reactive than tantalum – may influence the nucleation of chromia, with as result more Cr_2O_3 crystals per surface unit area. Indeed, Hf probably oxidized prior to chromia and tantalum on surface and the obtained hafnium oxides possibly acted as nucleation sites for chromia.
In addition, on the latter figure one can notice the presence of some dispersed small bright oxides. These ones are certainly oxides of tantalum or of hafnium. They represent a too small fraction to be detected by XRD and their too small size cannot allow specifying them accurately.

Cross–sectional observations
After cutting, embedding and polishing the two halves of the oxidized samples were observed in cross–section. Four SEM/BSE micrographs illustrate the observations, in Fig. 12. On the general views one can see that the external oxide scale – mostly composed of chromia (dark grey) – covers almost all the surface, despite some small parts necessarily lost during the metallographic preparation despite the nickel shell electrolytically deposited. This scale is a little irregular and a little porous. On the detailed views one can see that internal oxidation occurred in the subsurface close to the oxide scale / alloy interface. The pale oxides formed here, obviously often in contact with the inner side of the chromia scale, are obviously a mix of a complex oxide of tantalum and hafnium, as suggested by the X-maps presented as examples in Fig. 13 ("Ta > Hf" alloy) and in Fig. 14 ("Hf > Ta" alloy). In contrast with many cast superalloys containing interdendritic carbides for mechanical resistance purpose there is seemingly no carbide–free zone

which developed inwards from the scale / alloy interface, despite the rather high temperature of oxidation. In fact carbides really disappeared but under the effect direct oxidation, without real disappearance of the carbides for releasing carbon and carbide–forming metal and diffusion of these species towards the oxidation front. Here, even for the "Ta > Hf" alloy, there is more the in situ conversion of carbides in oxides than carbide dissolution followed outward diffusion which occurred. This behavior is closer to the HfC–strengthened alloys one [16] than to the TaC–reinforced alloys one [17]. Consequently, Ta did not diffuse and form a $CrTaO_4$ oxide at the interface and thus did not favor the spallation at cooling of the external scale as it did for TaC–reinforced alloys [17].

Concentrations profiles were acquired in the subsurface of the two oxidized alloys (Fig. 15). One can see that chromium diffused from more than 150µm for the "Ta > Hf" alloy but from only a little more than 100µm for the "Hf > Ta" alloy. Tantalum, present in the matrix with a higher content for the "Ta > Hf" alloy than for the "Hf > Ta" alloy, diffused from a little more than 100 µm for the "Ta > Hf" alloy, diffusion depth significantly higher than the one for the "Hf>Ta" alloy (≈ 50 µm). Concerning Hf, it is almost absent in the matrix and no gradient concerning it was noted.

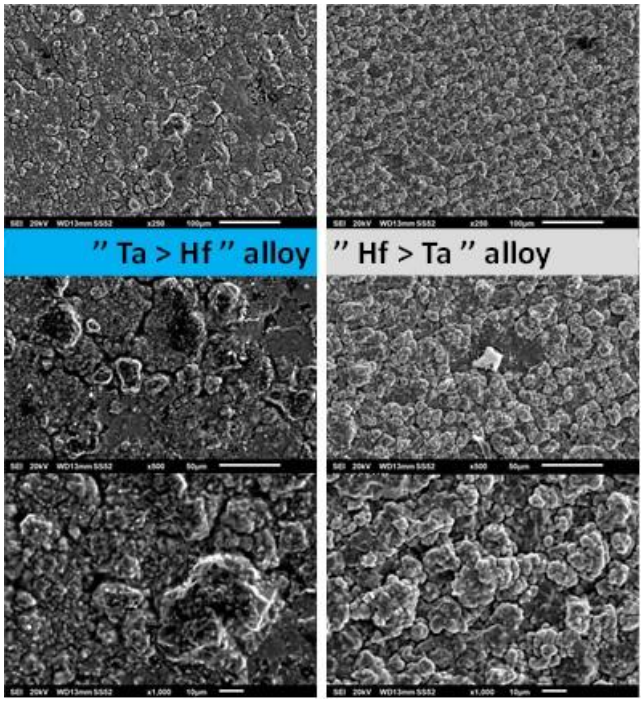

Fig. 10. Imaging of the gold–coated oxidized surfaces of both alloys: "Ta > Hf" alloy (left) and "Hf > Ta" alloy (right); general view (×250, top) and two more detailed views (×500, middle) and (×1000, bottom); WF–SEM in SE mode.

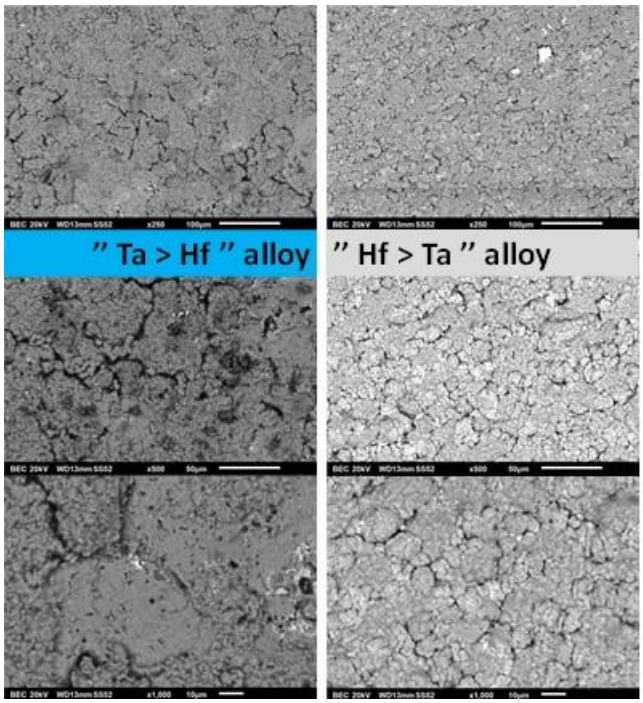

Fig. 11. Imaging of the gold–coated oxidized surfaces of both alloys: "Hf > Ta" alloy (left) and "Hf > Ta" alloy (right); general view (×250, top) and two more detailed views (×500, middle) and (×1000, bottom); WF–SEM in BSE mode.

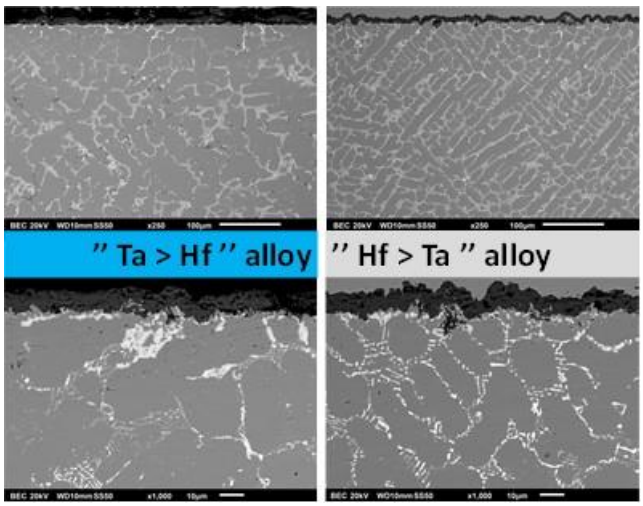

Fig. 12. BSE imaging (WF–SEM) of the oxidized surfaces and subsurfaces of the two alloys "Ta > Hf" (left) and "Hf > Ta" (right); general view (×250, top) and detailed view (×1000, bottom); WF–SEM in BSE mode.

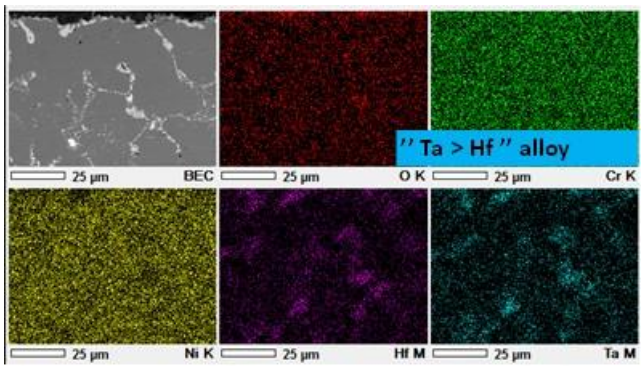

Fig. 13. EDS X-maps acquired somewhere in the oxidation–deteriorated subsurface of the "Ta > Hf" sample; WF–SEM EDS device.

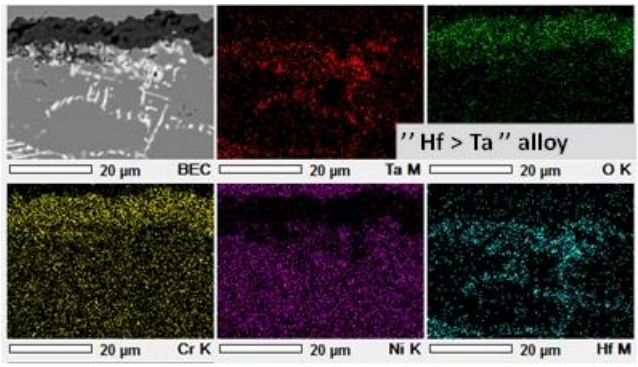

Fig. 14. EDS X-maps acquired somewhere in the oxidation–deteriorated subsurface of the "Hf > Ta" sample; WF–SEM EDS device.

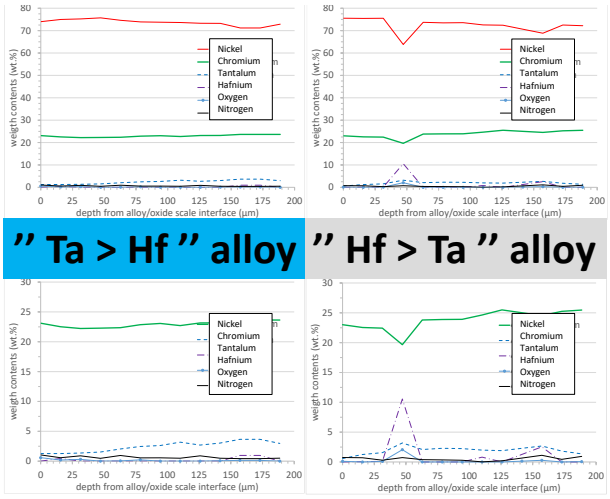

Fig. 15. EDS concentration profiles from the external oxide scale / alloy interface towards the bulk, measured in the "Ta > Hf" alloy subsurface (left) and in the "Hf > Ta" alloy subsurface: all elements (top) and enlargement for the elements in low concentrations (bottom); WF–SEM EDS device.

Bulk microstructure changes

The microstructures of both alloys after their exposure to 1100°C during 50 hours were also examined. The high magnification micrographs presented in Fig. 16 show that of the two alloys did not evolve significantly. The Chinese–script morphology of the MC carbides were not affected. One can just notice that secondary MC precipitation took place in the matrix, close to the interdendritic spaces.

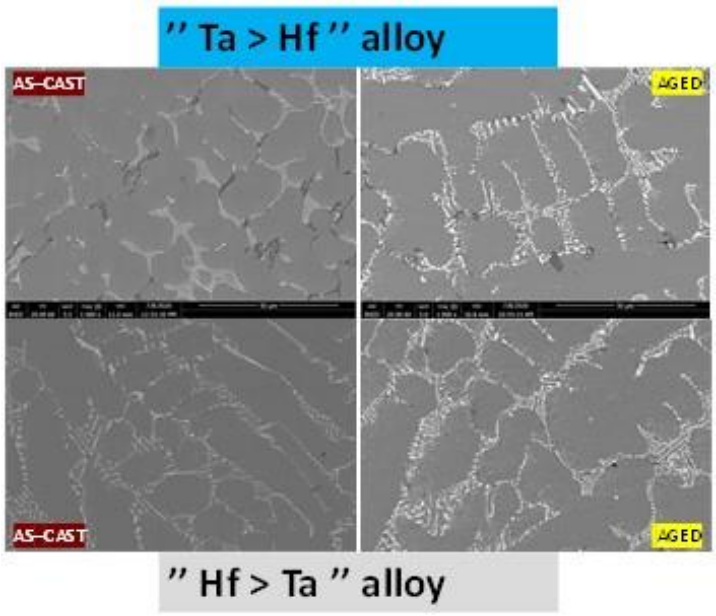

Fig. 16. The initial (left) and aged (right) microstructures of the "Ta > Hf" (top) and "Hf > Ta" (bottom) alloys (FEG–SEM in BSE mode, ×1000).

Bending creep deformation

The creep deformation kinetic were analyzed for both alloys. The obtained results are displayed in Table 1. The two alloys resisted rather well against deformation under constant load despite the test temperature particularly high (1100°C) for such conventionally cast nickel alloys reinforced by carbides. With less 5 µm / h of displacement of the central point (where the load was applied), the creep deformation was remarkably low taking into account the high level of the test temperature. After 50 hours the central movement was less than 0.5 mm in both cases. Obviously, the MC carbides and their resistance against morphology evolution strengthened the alloys efficiently.

The creep performances are only a little worse than for a HfC–reinforced Ni–based alloy earlier studied (same apparatus and sample geometry and dimensions, 1100°C–20MPa: 2.5µm/h and 0.27mm of central deformation.

Table 1. Results of the bending creep tests of the two alloys (1100°C, 20MPa).

Parameters	Alloys	
	"Ta > Hf" alloy	"Hf > Ta" alloy
Central point displacement rate at t = 50 hours	2.96 µm h^{-1}	4.76 µm h^{-1}
Deformation at 50 hours	231 µm	439 µm

Conclusion

Introducing less hafnium and replacing the missing Hf part by tantalum does not completely change the high temperature and creep performance of an alloy initially designed to be HfC–reinforced. The oxidation behavior and the creep resistance stay at a very high level: low oxidation rate due to the chromia–forming behavior, excellent resistance to oxide scale spallation at cooling, low deformation rate under the effect of a constant load. The performances are a little lower than for a nickel–based alloys reinforced by the same MC carbides quantity but only made of HfC but still much higher than an alloy only reinforced by TaC and chromium carbides. With less Hf, the production cost can be significantly lowered by involving smaller quantity of this expensive and not easily available element. As outlooks one can think now to test these alloys for longer durations and also at temperatures a little higher (1150 and even 1200°C). Another prospect is also looking for an intermediate Ta/Hf balance allowing a carbide population made of HfC only, but with a Ta content and a Hf content respectively lower and higher than in the "Hf >Ta" alloy.

References

[1] Donachie M.J., Donachie S.J., *Superalloys: A Technical Guide* (2nd Edition), ASM International, 2002.
[2] Young D.J., *High Temperature Oxidation and Corrosion of Metals*, Elsevier, 2008.
[3] Hopgood A.A., Martin J.W., (1986) *Materials Science and Engineering*, **82**, 1986, p 27–36.
[4] Zhao X., Liu L., Yu Z., Zhang W., Fu H., *Materials Characterization*, **61**, 2010, p. 7–12.
[5] Cui L., Su H., Yu J., Liu J., Jin T., Sun X., *Materials Science and Engineering A*, A696, 2017, p. 323–330.
[6] Cui L., Su H., Yu J., Liu J., Jin T., Sun X., *Materials Science and Engineering A*, A707, 2017, p. 383–391.
[7] Michon S., Aranda L., Berthod P., Steinmetz P., *Revue de Métallurgie – C.I.T./Science et Génie des Matériau*, 101, 2004, p. 651–662.
[8] Berthod P., Aranda L., Vébert C., Michon S., *Calphad*, **28**, 2004 p. 159–166.
[9] Berthod P., Michon S., Aranda L., Mathieu S., Gachon J.C., *Caphad*, **27**, 2003, p. 353-359.
[10] Berthod P., *Journal of Alloys and Compounds*, 481, 2009, p. 746–754.
[11] Berthod P., *Materials Science: An Indian Journal*, **9**, 2013, p. 359–365.
[12] Berthod P., Conrath E., *Journal of Material Science and Technology Research*, *1*, 2014 p. 7–14.
[13] Conrath E., Berthod P., (2018) *Materials Science*, **53**, 2018, p. 861–867.
[14] Lang D., Pöhl C., Holec D., Schatte J., Povoden-Karadeniz E., Knabl W., Clemens H., Primig S., *Journal of Alloys and Compounds*, 654, 2016, p. 445–454.

[15] Zhang J., Tian Y., Zhu J., Sun Y., Luo G., Shen Q., Zhang L., *International Journal of Refractory Metals and Hard Materials*, **86**, 2020, 105096.
[16] Conrath E., Berthod P., *Oxidation of Metals*, 81, 2014, p. 393–405.
[17] Berthod P., Vébert C., Aranda L., *Journal of Materials Science*, **42**, 2007, p. 352–362.